DOI: https://dx.doi.org/10.4314/gjgs.v19i1.1

GLOBAL JOURNAL OF GEOLOGICAL SCIENCES VOL. 19, 2021: 1-14
COPYRIGHT© BACHUDO SCIENCE CO. LTD PRINTED IN NIGERIA ISSN 1596-6798
www.globaljournalseries.com, Email: globaljournalseries@gmail.com

GEOPHYSICAL INVESTIGATION OF THE ORLE RIVER FRACTURE SYSTEM IN IGARRA TOWNSHIP, SOUTHWESTERN NIGERIA

MUSLIM B AMINU

(Received 24 January 2019; Revision Accepted 13 June 2019)

ABSTRACT

The subsurface structure and propagation geometry of the fracture system controlling the Orle River Channel in the Igarra Township, Southwestern Nigeria, have been investigated via a multi-method geophysical survey. The goal was to delineate the nature, distribution, and spatial propagation geometry of the fracture system and evaluate its potential to serve as storage and distribution features for groundwater within adjoining areas. 2D electrical resistivity, total field magnetic, and co-planar loop conductivity measurements were collected along four traverses using an ABEM1000 Terrameter unit, a GEMS Magnetometer, and an EM34 Co-planar loop electromagnetic system. Traverses were established to run across and parallel to the river channel. The observed electrical resistivity field data were inverted for subsurface 2D resistivity structure using a commercially available 2.5D finite element modelling inversion software. Magnetic field intensity data and ground conductivity data were presented against station positions. Three subsurface layers were delineated at the survey site; (1) surficial humus-rich and wet top-soil, (2) a thin poorly developed weathering layer, and (3) the fresh bedrock which occurs as relatively shallow levels and often outcrops. The River channel is controlled by multiple fractures usually located at or near the contracts between contrasting rock types. Fracture dip is usually in the northerly direction but conjugates, dipping southwards also occur in the most northerly extremes of the imaged fracture system. Upstream the fracture path is wider and along with the imaged overburden, is juxtaposed northwards of the channel axis suggesting a much broader river channel in the geologic past. Low aperture fractures imaged tangential to channel axis likely serve to funnel surface and groundwater from the channels to the surrounding areas. Where such low aperture fractures can be delineated, they offer the best chances of groundwater abstraction within adjoining areas, particularly during the dry season.

KEYWORDS: Igarra Township, subsurface resistivity structure, fracture geometry, bedrock structure, ground electrical conductivity.

INTRODUCTION

The Orle River is a seasonal stream channel situated within a major open-to-surface fracture system. It segments the Igarra Township into a small northern segment and a much larger southern segment (Figure 1). The system consists of a main channel running in the east-to-west direction and few short length distributaries which branch off often at right angles to the main channel. The channel takes its source from high rising granitoid hills east of the town and tails off west of Igarra in extensive flood plains with the development of considerable meanders. It is the main source of water for locals almost all-year-round. In the dry season, this river though with much-diminished volume becomes the only source of water for locals and herded cattle within the northern parts of the town. This paper presents the results of a multi-method geophysical survey aimed at unraveling the geometry of the underlying fracture system beneath the Orle river channel and its potential for groundwater storage and distribution.

Geophysics tools enable the investigation of subsurface geologic structure in a rapid and cost-effective manner (LaBrecque et al., 1996; Zume et al., 2006; Frid et al., 2007; Lines et al., 2012; Aminu et al., 2014, 2015a & b; Aminu, 2018). They provide non-invasive sensing of rock properties with a reasonable trade-off between cost and accuracy. They enable rapid and detailed screening for groundwater (Zume et al., 2006; Frid et al., 2012; Mohamed et al., 2012). In construction site investigations, they offer semi-continuous and sometimes continuous profiling of structures inimical to civil works projects (Soupios et al., 2002; El-Qady et al., 2005; Chavez et al., 2014; Yassin et al., 2014; Aminu, 2018). They also provide information on the morphology and spatial distribution of underlying geologic features (Aminu, 2015a), the nature and thickness of the overburden and depth to competent bedrock or formations (Robineau et al., 2007), groundwater regimes (Rizzo et al., 2004; Bufford et al., 2012; Aminu et al., 2014) and ground corrosivity (Ekwe et al., 2018). They sometimes provide quantitative estimates of in situ

Muslim B. Aminu, Department of Earth Sciences, Adekunle Ajasin University, Akungba-Akoko, Nigeria.

geotechnical properties (Anderson, 2006; Cosenza et al., 2006) of the subsurface geologic strata and clues to the tectonic history of surveyed areas (Bufford et al., 2012; Aminu et al., 2014).

Bufford et al., (2012) imaged the geometry and nature of fault activity along the Okavango Rift Zone in Botswana in the southwestern branch of the East African Rift System. The rift zone was delineated as a low resistivity path which was interpreted to channel both surface water and groundwater from the Okavango delta and re-circulating it through lacustine and fluvio-deltaic sediments of the basin. El-Qady et al., (2005) employed ground-penetrating radar and electrical resistivity imaging to reveal the subsurface structure of a Karst cave over a proposed site for low-income residential apartments in the eastern parts of greater Cairo. Previously unknown extensions of the cave system were delineated as zones of marl, and multiple vertical fractures in limestones. Aminu et al., (2014), employed electrical resistivity imaging to delineate the Uneme-Nakhau fracture zone. The fracture zone was imaged as consisting of two distinct fractures where deformation had ceased on one fracture and had been transferred to the other. Park and Roberts, 2003, utilize prior magnetotelluric (MT) data and electrical resistivity, and formation factor data from core plugs of sedimentary rocks within the San Andreas Fault to offer an alternative interpretation of MT data presented in Unsworth et al., 1997. They aver that the anomalous region results from conductive sedimentary rocks within the plunging syncline adjacent to the fault rather than fractured rock.

GEOLOGICAL SETTING

Igarra Township is situated in Akoko-Edo local government area of Edo State, Nigeria, between Longitudes 05˚ 43' and 05 ˚ 47', and Latitudes 07˚ 27' and 07˚ 31' (Figure 1). It situates within the Igarra schist belt of the basement complex of southwestern Nigeria, a region consisting of predominantly of migmatitic and granitic gneisses (Rahaman, 1989). The Igarra schist belt is regarded as the best known of the most easterly schist belts in Nigeria which are distributed around the Okene migmatitic nucleus (Turner 1989). Physiographically, the area consists of a westward Drainage is provided by a number of seasonal streams which take their source from high reliefs in the east and empty west of the town.

In the Igarra region, the main geological structure is an open synform which refolded in east-west folds. In this mini-basin, metamorphosed calcareous rocks and conglomerates occur along with quartzites as steeply dipping bands in the dominant biotite gneiss (Turner, 1989). Older migmatites form the periphery around the synform. Late-stage intrusives include porphyritic-granite, aplite/pegmatite, syenite, and subsidiary quartz vein. Multiple deformation episodes are recognized in the area bringing together a diverse blend of metamorphic and igneous rocks. Extensive folds and abundant fractures characterize the area. The details of the geologic associations and structural development of the area can be found in (Odeyemi 1988; Annor 1998; Ogbe et al., 2018). Figure 2 is a geologic section showing the typical geologic relationship in the southern parts of Igarra.

STUDY SITE

This survey was carried out around the Orle River Channel at a section of the River running in the ENE-WSW direction for roughly 450 m (Figure 1d). The channel pass is dotted with thick vegetation while the surrounding plains are cultivated by locals during the long wet season. The site is underlain by low-lying quartzite outcrops to the north and northwest. Metaconglomerates occupy the south, southwest, and part of the northeast with low-lying outcrops to the north of the channel. South of the channel, metaconglomerates rise a few meters above the ground surface. The eastern part of the study area is underlain by Phyllites which can be seen outcropping at two sites on the eastern side and within the channel bottom of a N-S trending tributary of the Orle River channel. Fault breccias occur on the ground surface on the northern side of the Channel. The body is elongate with a total length of ~130 m and a thickness of up to 20 m. It has a strike parallel to the course of the channel in the ENE-WSW. The channel is fully accessible during the dry season through footpaths which intercept it at two crossings frequently utilized by locals. In the extreme southeastern part of the area, sparsely located settlements occur. The study site covers an area roughly 100,000 m^2.

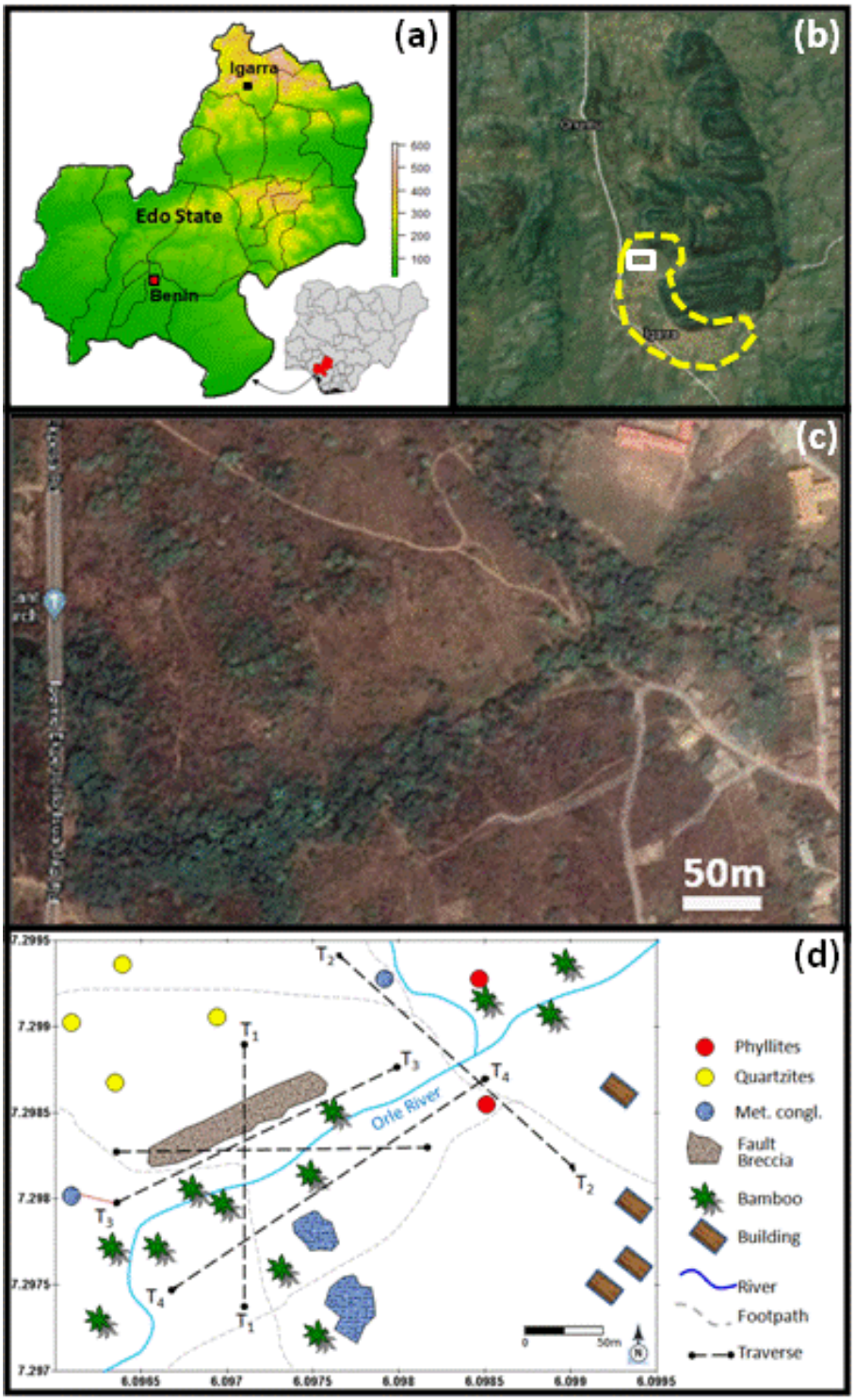

Figure 1: Composite panel of the study area: (a) Map of Edo State; (b) Satellite map of Igarra (Google map, 2018); (c) Satellite map of the Orle channel dotted with thick vegetation (Google map 2018); (d) Study site with traverses and major features.

METHODOLOGY

Data Collection

Four (4) traverses were established and surveyed within the study area. (Figure 1d shows the spatial relationships between the traverses and natural features). Traverse 1 (T_1) spanned a total length of 200 m and ran in the southeast to northwest direction crossing the Orle River channel at its northern end within the study area. This point is a popular stream crossing for locals and therefore easily accessible. Traverse 2 (T_2) spanned a length of 170 m and ran in a south to north course, first across the Orle River channel, then across an inferred contact between metaconglomerates and quartzite facies, and then over a surface occurrence of fault breccias. Traverses 3 and 4 (T_3 & T_4) both ran in the northeast to southwest direction roughly parallel to the trend of the Orle River channel. Traverse 3 was 200 m long and ran between the channel and the fault breccias. It crossed T_2 at about its 110 m mark and terminated close to a flat-lying metaconglomerate outcrop. T_4 ran roughly 5 m from the edge of the southern flank of the River channel and

intersected T_1 at its northern end. T_4 runs from a region with outcropping Phyllites in its northern end to metaconglomerates in its southern reaches. Data collected included 2D Electrical resistivity, Total Field Magnetic Intensity, and ground Electrical Conductivity.

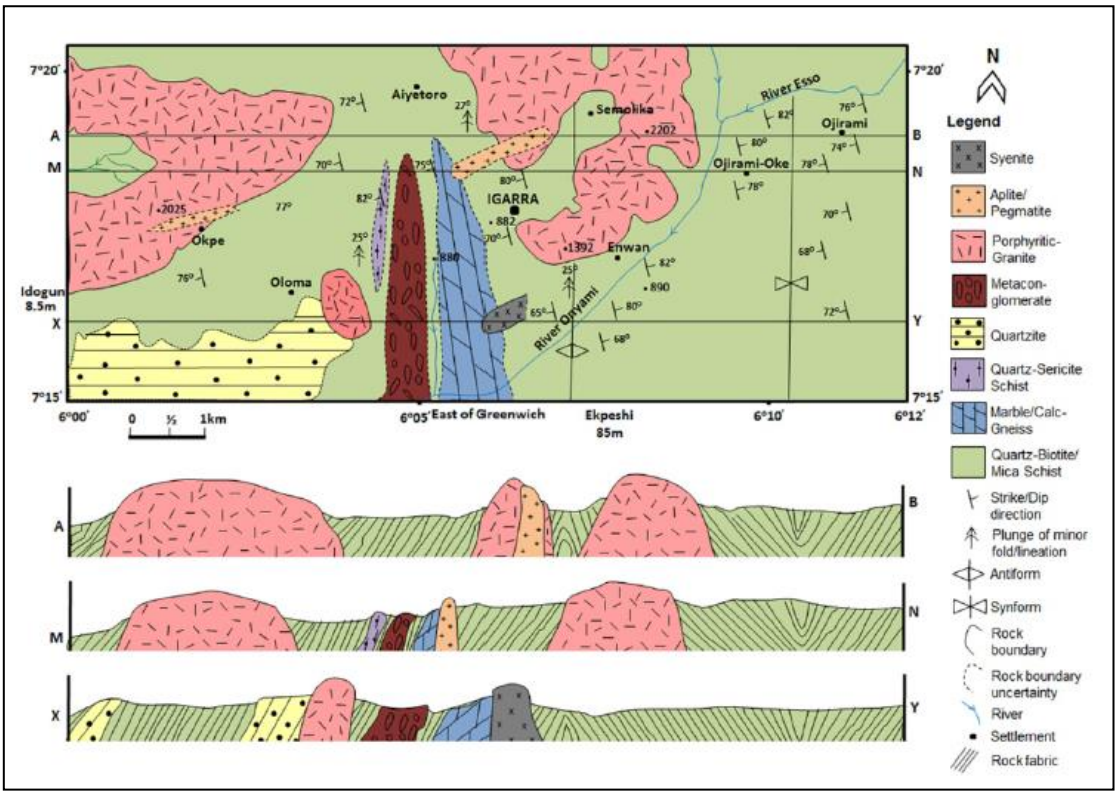

Figure 2: Typical geological associations within the study area: geologic map (top), cross-section (bottom). Alternating bands of meta-sedimentary rocks are frequently intruded by granitic plutons.

The electrical resistivity data were collected using the ABEM 1000 Terrameter system. The dipole-dipole electrode configuration was employed on all traverses to capture lateral as well as vertical variations in conditions of the subsurface. Dipole spacing on T_1 was 10 m and a maximum dipole length of 70 m was achieved. On T_2, T_3, and T_4, dipole spacing was maintained at 5 m and a maximum dipole length of 40 m was achieved in each case. Total magnetic field intensity measurements were collected on all traverses using the GEMS System Magnetometer. Data were collected at 5 m spacing on T_1 and T_2 and 2 m spacing on T_3 and T_4. Ground electrical conductivity data were collected at 5 m intervals along all traverses using the Geonics Coplanar loop EM34 system. A coil separation of 10 m was utilized. Data were collected in March 2017, just at the onset of seasonal rains.

DATA PROCESSING

Acquired ground resistivity data were evaluated for spikes and data inversion was carried out using DIPROfWIN 4.0.1, a 2.5D finite element modelling inversion algorithm described in Yi and Kim, (1998). The program utilizes the Active Constraint Balancing scheme to determine the spatially varying Lagrangian multipliers for the least-squares inversion algorithm in a bid to optimize between robustness and smoothness of the inversion. The program computes an initial synthetic subsurface resistivity distribution model and then attempts to minimize the difference between it and the observed resistivity fields until a reasonable fit is achieved. The inversion is deemed suitable and the iteration is stopped once the mismatch error drops below 5%. The program output three images, the observed field data pseudo-section, the computed theoretical data pseudo-section, and the inverted subsurface resistivity structure. Considering the wide range of inverted resistivity (0 – >20000 Ohm-m) a logarithmic colour display was utilized and the display was limited to the range 89 – 6000 Ohm-m as this provided the best visual representation of resistivity distributions along the traverses. Topographic variations were factored in during the inversion process for T_1 and T_2. T_3 and T_4 required no topographic corrections as they were flat. Total magnetic field (TMI) intensity data were smoothened for spikes and reduced using a regional 32500 nT background. The Residual magnetic intensity (RMI) values were presented along the traverses. Electrical conductivity measurements were simply presented along traverses.

INTERPRETATION CRITERIA

Interpretation criteria for resulting 2D subsurface resistivity structure of the subsurface followed similar criteria to that utilized in Aminu et al. (2014), Aminu (2015a), and Aminu (2015b). High laterally and or vertically continuous resistivities in the subsurface and at depth (usually above 1000 Ohm-m) were interpreted

to indicate unfractured bedrock. Low and shallow continuous-in-the-subsurface resistivities (usually below 150 Ohm-m) were interpreted to represent water-saturated surficial humus and clay-rich top-soil. Resistivities ranging from 160 – 900 Ohm-m were interpreted as partly weathered bedrock and or conductive fracture paths depending on the lateral and vertical continuity and geometry of the imaged responses. Further, interpretations of the geophysical responses from all data were constrained by the geological information afforded by the geological setting and rock outcrops within the area.

RESULTS

Figure 3 provides a composite view consisting of plots of the inverted 2D subsurface resistivity response beneath T_1 and the corresponding electrical conductivity and residual magnetic intensity responses. The 2D resistivity response consists of three distinct patterns. A first response pattern, high resistivity responses (>1000 Ohm-m), occurs continuously at depth all through the section. Generally, the upper limits of this response pattern occur at 2 – 4 m depth. However, the pattern nearly reaches the surface at 40 – 50 m and 60 – 70 m. In the northern extremes of the traverse, this pattern reaches the surface. Outcropping Phyllites occur west of this traverse at the 60 – 70 m mark. East of the northern end of the traverse, a low-lying metaconglomerates outcrop occur. The upper limit of this pattern also forms a trough between 80 m and 150 m. Beneath this trough region, the high resistivity pattern presents with much lower responses relative to the rest of the traverse and appears to separate the high resistivity response pattern into two segments. Low resistivity responses (<150 Ohm-m) occur at the surface at 90 – 130 m reaching a maximum depth of ~ 6 m. This pattern sits within the trough on the upper limit of the high resistivity pattern and is largely coincident with the Orle River channel at 85 – 105 m. On this traverse, intermediate resistivity responses (160 – 900 Ohm-m) occur in the near-surface of the southern end of the traverse (18 – 36 m and 50 – 60 m) and as a generally thin layer underlying the low resistivity responses within the trough region. They separate the high resistivity and low resistivity responses. The residual magnetic anomaly response varies from 452 nT to 808 nT. A clear asymmetric magnetic anomaly occurs in the middle of the traverse (90 – 100 m).

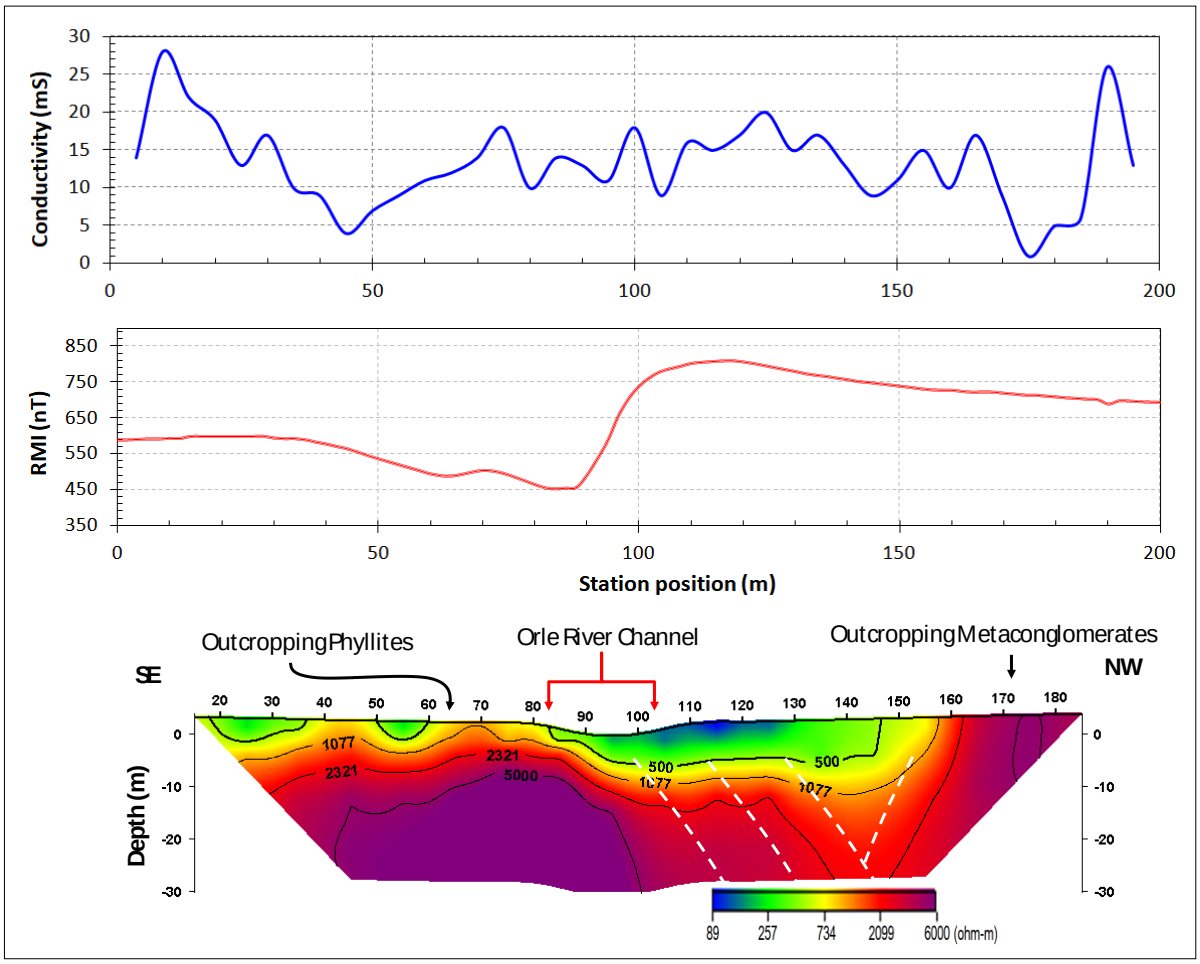

Figure 3: Composite panel of 2D subsurface resistivity image, residual magnetic intensity, and ground electrical conductivity response along Traverse 1. A wide fracture path is indicated slightly north of the channel but directly below relatively extensive low resistivity responses. White dashed lines indicate inferred fractures.

The inflection point on this anomaly is approximately coincident with the location of Orle River channel. The conductivity response oscillates in no systematic pattern from 1 – 28 mS.

Figure 4 provides a composite view consisting of plots of the inverted 2D subsurface resistivity response beneath T_2 and the corresponding electrical conductivity and residual magnetic intensity responses. The 2D resistivity response also consists of three distinct patterns. The first pattern occurs as shallow and relatively laterally continuous very-low resistivity responses with values generally less than 150 Ohm-m. For most of the traverse, this response pattern extends from the ground surface to depths hardly exceeding 4 m. The exception is between 30 m and 90 m where it is replaced by considerably higher resistivity responses. The second pattern consists of very-high resistivity responses with resistivity values greater than 1000 Ohm-m. This response pattern is fairly continuous at depth within the subsurface and extends from depths as shallow as 2 – 4 m below the ground surface till the bottom of the image. This high response pattern consists of two segments; 1) a southern segment which extends from the southern end of the traverse till the 70 m marks and whose upper surface is undulating. This segment is coincident with a region with known outcrops of metaconglomerates and; 2) a northern segment that extends from the 80 m mark till the northern limit of the traverse which has a gently humped upward surface. This segment is coincident with a region with outcropping quartzites. The lateral limits of the two segments beneath the river are defined by nearly vertical edges. In the subsurface, the separation between the two segments consists of much lower resistivity responses which lie in a vertical zone beneath the location of the Orle River channel at ~70 – 80 m. In this region, the high resistivity responses show much lower values (1000 – 1500 ohm-m) compared to the rest of the segments where values are generally above 2000 Ohm-m. Furthermore, adjacent to the 'cliff-edge' terminations, the two segments have concave upward trough-like depressions on their upper limits. The third response pattern has intermediate resistivity values in the range of 160 – 900 Ohm-m. At shallow depths, it spread out lateral at the surface occurring from 30 m to 90 m along the traverse and extending to depths of 2 – 5 m below the ground surface. At other places, it fills the intervening space between the low and high resistivity responses. At greater depths (>5 m) it separates the southern and the northern segments of the high resistivity response pattern in a narrow vertical zone between 70 m and 80 m. The residual magnetic anomaly response over this traverse varies from 463 nT to 667 nT. A relatively low response (460 – 470 nT) is indicated at 45 – 70 m along the traverse. This region coincides roughly with the location of Orle River. Magnetic responses at the southern end of the traverse are generally higher than at the northern end. The conductivity response is generally flat (10 – 30 mS). The exception is the 40 – 55 m mark where conductivity values reach 120 mS. This anomaly is located slightly south of the edge of the Orle river channel.

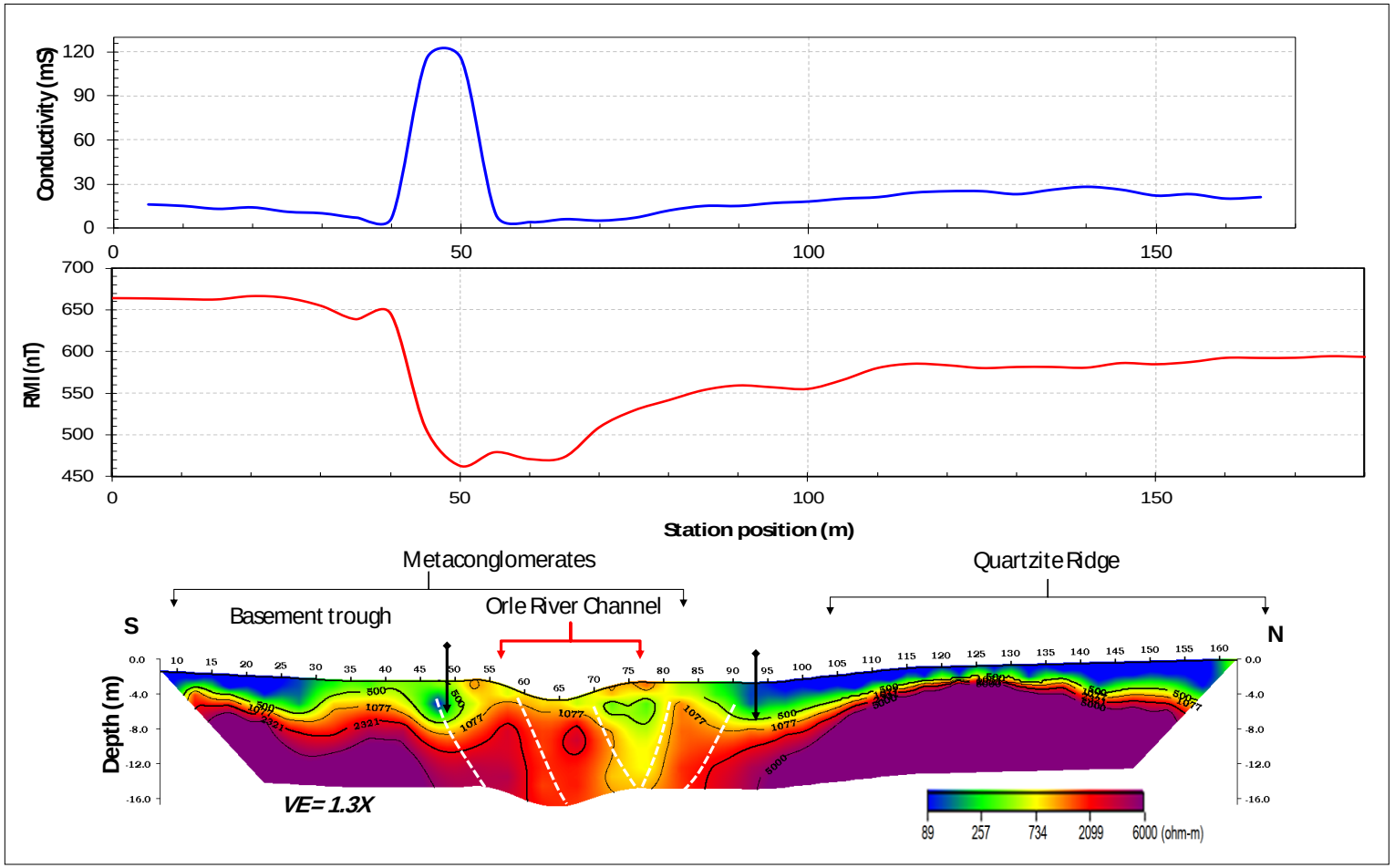

Figure 4: Composite panel of 2D subsurface resistivity image, residual magnetic intensity, and ground electrical conductivity response along Traverse 2. A much lower resistivity response spans from 50 – 90 m separating the high resistivity response into northern and southern segments. Bedrock topology is undulating south of the Orle channel but relatively smooth north of the channel. White dashed lines indicate inferred fractures.

Figure 5 is a composite view consisting of plots of the inverted 2D subsurface resistivity response beneath traverse 3 (T_3) and the corresponding electrical conductivity and residual magnetic intensity responses. Low resistivity responses (<150 Ohm-m) occur nearly all-through the traverse at shallow depths and outcrop between the 15 – 25 m, 43 – 53 m positions, and from 85 m to the western end of the traverse. This pattern, though better developed than one T_1 and T_2, rarely exceeds a depth of 4 m. The exception is at 50 – 65 m marks where it reaches a depth of 6 m. High resistivity responses (>1000 Ohm-m) occur nearly all-through at depth. The upper limit of this response occurs at depths as shallow as 2 m in the western end to as deep as 5 m in the eastern limits of the traverse. It is segmented into three units by vertical lower resistivity responses which occur at 57 – 67 m and 110 – 120 m. The top of the most easterly segment is relatively smooth while the other two segments are more rugose. Intermediate resistivity responses (160 – 900 Ohm-m) occur at the surface at 30 - 45 m and 55 -85 m and at depth at 57 – 67 m and 110 – 120 m. The residual magnetic anomaly response varies from 413 nT to 767 nT. The plot exhibits a broad depression with the highest field strengths located in the eastern limits of the traverse. The conductivity response oscillates rapidly in the range of 33 – 45 mS.

Figure 6 is a composite view consisting of plots of the inverted 2D subsurface resistivity response beneath traverse 4 (T_4) and the corresponding electrical conductivity and residual magnetic intensity responses. Laterally continuous low resistivity responses (<150 Ohm-m) occur along the traverse in the eastern limit of the traverse till the 24 m marks, at 40 – 128 m and 155 – 180 m. These responses extend from the surface to a maximum depth of 6 m between 155 – 180 m. High resistivity responses (>1000 Ohm –m) occur nearly all-through at depth. The upper limit of this response occurs at depths as shallow as 2 m in the western end to as deep as 5 m in the eastern limits of the traverse. In a similar fashion to T_1, T_2 & T_3, this response pattern is segmented by lower resistivity response at 30 – 35 m and 175 – 183 m. Its upper surface is undulating all-through. Intermediate resistivity responses (160 – 900 Ohm-m) occur at the surface at positions 22 – 40 m, 133 – 155m, 160 – 165 m and 180 m till the western end of the traverse and as a layer of responses separating the deeper high resistivity pattern from the shallow low resistivity pattern. It further occurs at depth at 30 – 35 m and 175 – 183 m, as two narrow vertical signatures. The most easterly surface occurrence of this pattern is laterally 5 m north of a low-lying outcrop of Phyllites. The magnetic response for the traverse ranges from 411 nT to 590 nT. For the 10 – 70 m marks, field responses are much lower (<500 nT) than for the rest of the traverse. From station 110 m, the curve is essentially flat till its western end. The conductivity response is generally flat at about 60 mS for most of the traverse. At positions, 125 – 135 m, 150 – 175 and 190 – 200 m, conductivity approaches zero.

DISCUSSION

Laterally continuous low resistivity responses (<150 Ohm-m) which generally occur within the first 4 m from the ground surface were interpreted to represent water-saturated surficial humus-rich soils at the site. High resistivity response patterns (> 1000 m) were interpreted as the unweathered bedrock in the area. In regions proximal to or directly beneath the Orle channel, sections of this pattern with resistivities in the range 1000 – 1500 Ohm-m are considered to be partly fractured. The intermediate

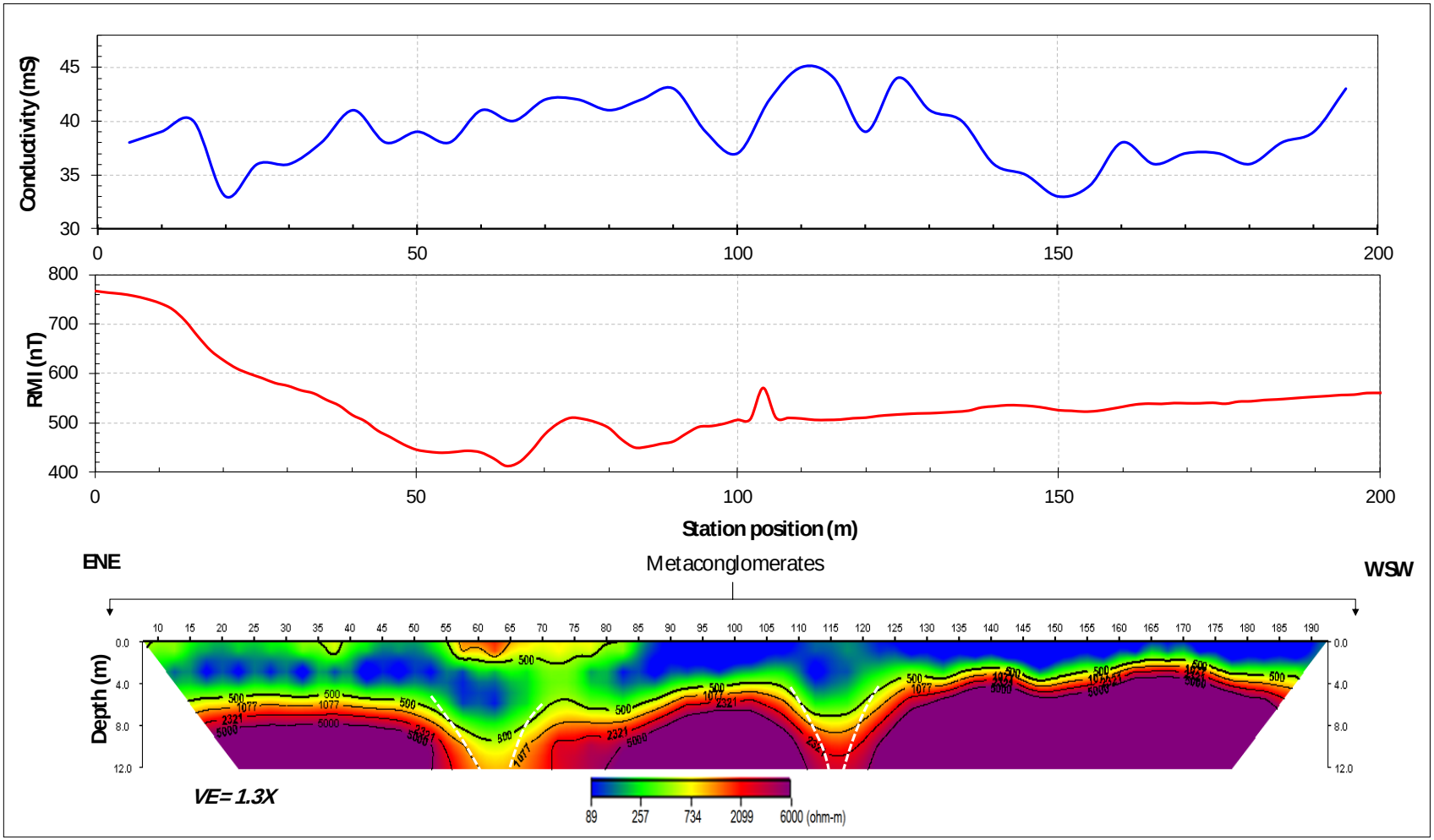

Figure 5: Composite panel of 2D subsurface resistivity image, residual magnetic intensity, and ground electrical conductivity response along Traverse 3. Low resistivity responses are laterally continuous within the subsurface till an average depth of 4 m. The entire traverse is suspected to be underlain by metaconglomerates. White dashed lines indicate inferred fractures.

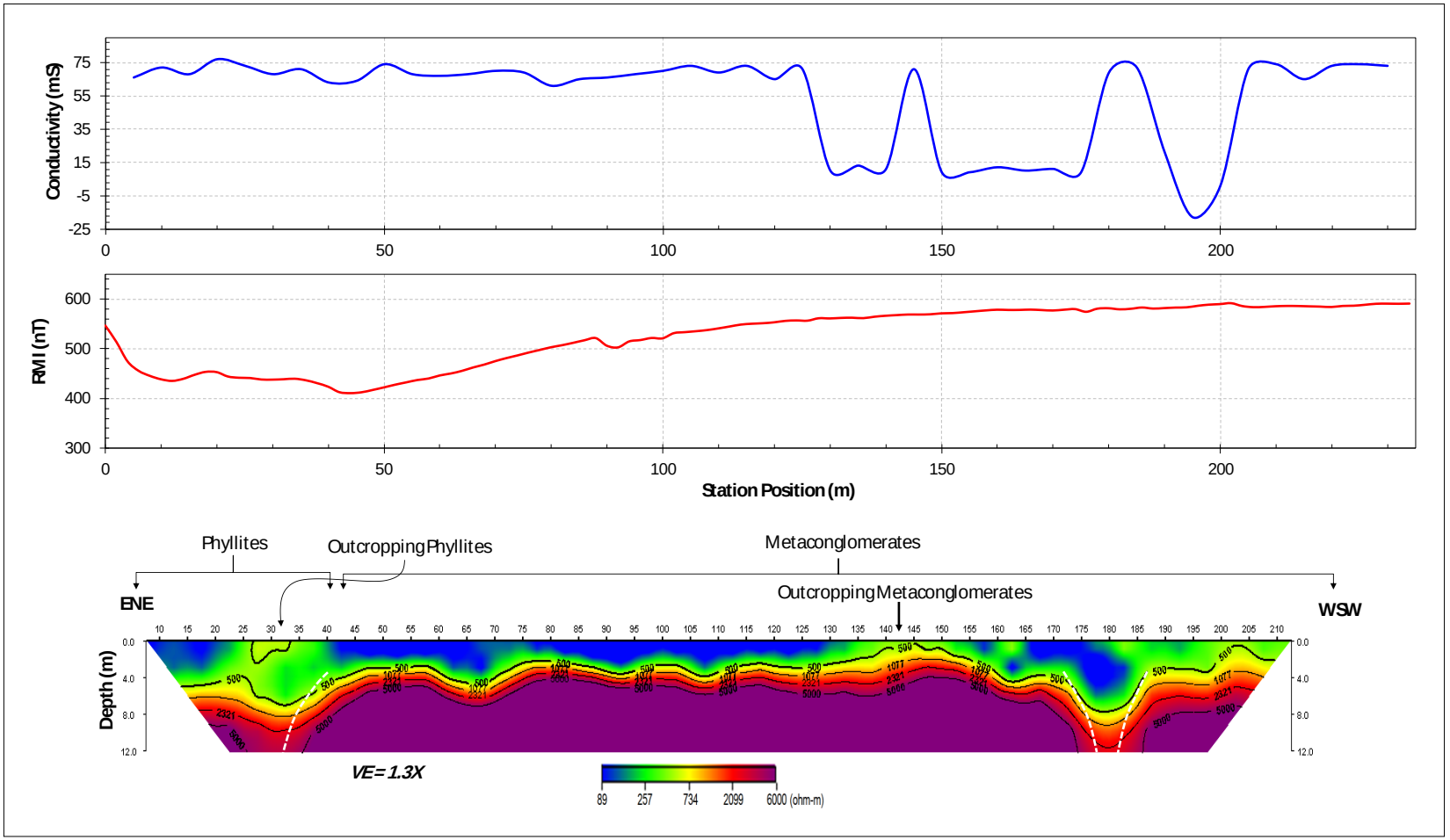

Figure 6: Composite panel of 2D subsurface resistivity image, residual magnetic intensity, and ground electrical conductivity response along Traverse 4. Low resistivity responses are laterally continuous within the subsurface and fill major troughs in the bedrock at the eastern and western end of the traverse. The eastern end produced a lowered magnetic response compared with the rest of the traverse. White dashed lines indicate inferred fracture.

resistivity response patterns (160 – 900 Ohm-m) were interpreted within shallow (2 – 6 m) sections as representing the zone of active weathering separating the topsoil from the unweathered bedrock. Deeper and vertical occurrences of this pattern were interpreted as highly fractured sections in the fresh bedrocks. The shapes of magnetic anomalies were used to infer the direction of dip of interpreted fractures beneath the channel. The electrical conductivity peak along T_1 was considered to suggest that the most southern of the interpreted fractures is conducting fluids within the subsurface and possibly has been active in recent times. Three subsurface layers are therefore delineated at the site; (1) the surficial humus-rich top-soil, (2) a thin weathering layer, and (3) the fresh bedrock. Together, the topsoil and the weathering layer form the overburden at the site.

The Orle river channel system is apparently fracture-controlled with multiple fractures interpreted beneath the channel axis on T_1 and T_2 (Figures 3 and 4). Judging from the inverted resistivity responses and the residual magnetic intensity response, most fractures beneath the channels axis have a northwards dip with only the most northerly fractures on both traverses acting as conjugates which dip in the southwards direction. On T_1, the fracture zone has a span of roughly 50 m (100 – 150 m) while on T_2 its span is about 45 m (45 – 90 m mark). This indicates a narrowing of the fracture zone downstream. Considering the spatial locations of rock outcrops (Figure 1c), the fractures appear to lie approximately along the contact zones between adjacent lithologies; between phyllites to the south and metaconglomerates in the north of T_1 and between metaconglomerates to the south and quartzites in the north of T_2. The north-trending tributary of the Orle channel also takes a path between known outcrops of metaconglomerates to the west and phyllites to the east. This can be expected as rock contacts are often zones of weakness in the bedrock and are more liable to brittle failure under the application of external stress regimes (Twiss and Moore, 2007). The channel for most of its course at the study site is probably constrained to run along the contacts between these lithologies. On T_1, interpreted fractures appear symmetrically distributed on both side of the channel. On T_2, they are rather displaced northwards of the channel.

Multiple fractures also appear to occur tangentially to the channel axis; these are observed on T_3 and T_4 (Figures 5 and 6). These are low aperture fractures generally less than 10 m in width. They encourage deep weathering of up to 8 m. On T_4, the eastern fracture possibly also takes advantage of the zone of weakness provided by the contact between phyllites to the east and metaconglomerates to the west.

Bedrock topography within the site is fairly rugose; undulating in most places underlain by metaconglomerates with the development of basement trenches which lie in close proximity to the 'cliff-edge' terminations of the bedrock (Figure 2). In regions underlain by quartzites, the bedrock topography is relatively smooth with convex upward surfaces (Figure 2). Apparently, the metaconglomerates within the area are more susceptible to weathering and possibly also fracturing relative to the phyllites and quartzites. Within the greater Igarra region, quartzites ridge rise above adjacent metaconglomerates.

Overburden development at the site is relatively thin, rarely exceeding 5 m below the surface. Exceptions occur in deep weathering zones created by fractures within the underlying fresh bedrock along T_3 and T_4, and at troughs atop the bedrock mostly in regions underlain by metaconglomerates (Figures 2, 3 and 4). Along T_1 (Figure 1), the overburden fills an extensive basin-like depression from 80 m mark to 155 m. Here the overburden is generally displaced north of the channel axis with its thickest section occurring from the 110 m marks onwards. The lowest resistivities (< 150 Ohm-m) are also largely juxtaposed north of the channel axis. Interpreted fractures along this traverse span a region coincident with this depression. Upon visual inspection along the Traverse, thick sand intervals were observed just north of the Orle channel and also within and on the banks of the north-trending tributary of the Orle channel system. This possibly indicates that a much wider channel existed at this location in earlier geologic times.

Figure 7 is the superposition of the field layout upon the derived conceptual model of the subsurface at the survey site for an average depth of 8 m beneath the ground surface. The north-western region of the study site is most likely underlain all-through by quartzites. This forms the most elevated part of the area. Phyllites possibly underlie the entire eastern region while metaconglomerates appear to occupy a band in-between the quartzites and phyllites which thins northwards and fans out in the south-westerly direction. This model of alternating bands of metasedimentary rocks agrees with geologic models earlier determined via field mapping within the greater Igarra area by Ogbe et al., (2018). The fault breccias occurrence appears to be a surface feature. Its specific origin has not been imaged within this study.

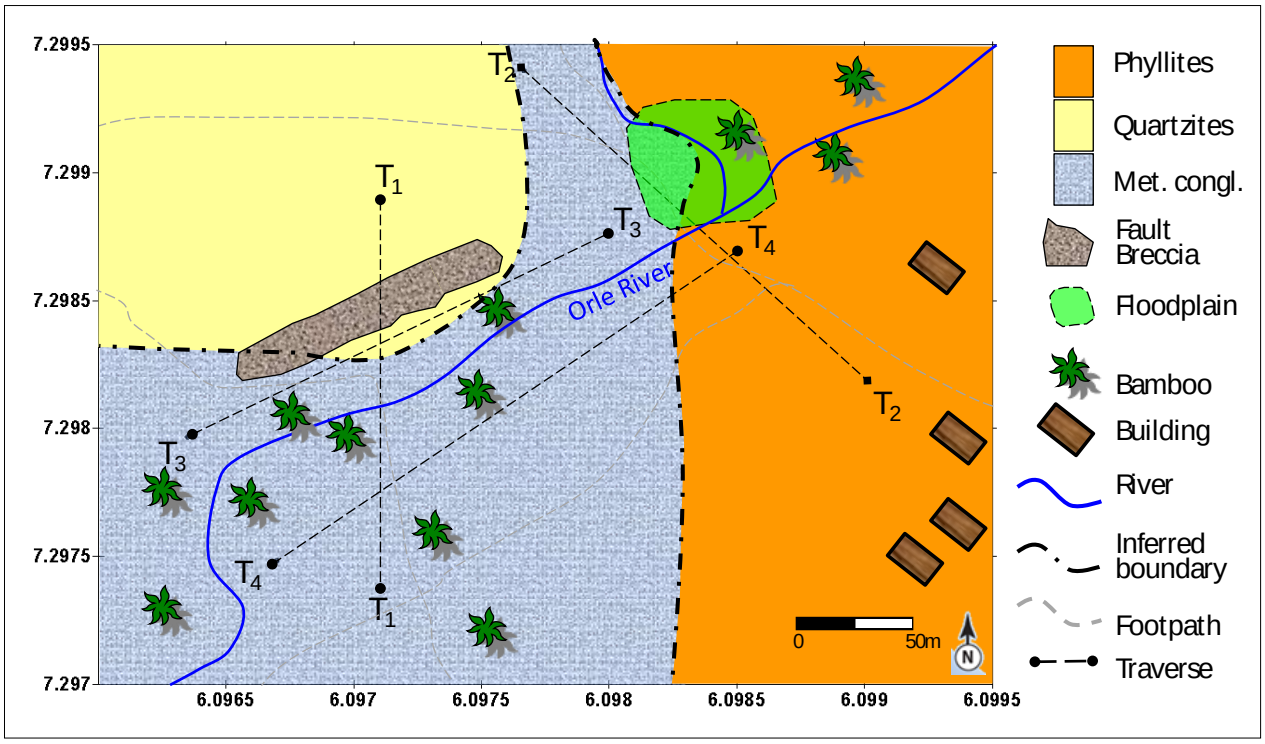

Figure 7: Conceptual geologic model at an average depth of 8 m below the surface at the study site. The lithologic distribution grades from quartzites in the northwest to metaconglomerates in the centrals part and phyllites in the eastern region.

It could however be expected to lie somewhere along the quartzite-metaconglomerate contact as the clasts within the breccias are considered to originate from the quartzite. Fractures tangential to the channels axis apparently serve to channel surface and groundwater from the channel to surrounding areas. If persistent they could serve as potential aquifers and distributors of groundwater to neighbouring areas.

CONCLUSION

In this study, we have used a combination of 2D electrical resistivity imaging, total field magnetic and ground conductivity data to unravel the nature and morphology of part of the subsurface beneath and around the Orle River system. The Orle river system and its tributaries are fracture controlled. The fracture system is complex and features multiple fractures including conjugates. Fracture development within the area is concentrated at weak zones at the contacts between contrasting lithologies and also within areas underlain by metaconglomerates, the metaconglomerates being more susceptible to brittle failure and weathering relative to other lithologies. Low aperture fractures that are tangential to the Orle Channels encourage relatively deeper weathering away from the channels axis. They could serve to funnel surface and groundwater from the channel system into more remote areas beyond the channel axis and its immediate surroundings. Overburden development is generally thin and insufficient for considerable groundwater storage and as such, hand-dug wells will only be viable within the wet season.

ACKNOWLEDGMENT

The author wishes to acknowledge the Tertiary Education Trust Fund (Tetfund) of the Federal Republic of Nigeria for support under the Institution Based Research Initiative (VC/APU/025). The author further acknowledges Adedibu Sunny, Adekunle Sadiq, and Mufutau Isiaka for field support.

REFERENCES

Aminu, M. B., Akande, T. M. and Ishola, A. O., 2014. 2D Geoelectric Imaging of the Uneme-Nekhua Fracture Zone. International Journal of Geophysics, http://dx.doi.org/10.1155/2014/842812

Aminu, M. B., 2015a. Electrical Resistivity Imaging of a Thin Clayey Aquitard Developed on Basement Rocks in Parts of Adekunle Ajasin University Campus, Akungba-Akoko, South-western Nigeria. Environmental Research, Engineering and Management, 71(1), 47 – 55.

Aminu, M. B., 2015b. Geo-electric Investigation of the Cause of Structural Failure Indices on a Set of Administrative Blocks. Journal of Applied Geology and Geophysics, 3(4), 1-10.

Aminu, M. B. 2018. Subsurface Electrical Resistivity Imaging and Electromagnetic Conductivity Profiling at a Proposed Construction Site at Adekunle Ajasin University Campus, Akungba-Akoko, South-Western Nigeria. Global Journal of Geological Sciences, 16, 53-60.

Annor A. E., 1998. Structural and Chronological relationship between the low grade Igarra Schist and adjoining Okene Migmatite-Gneiss terrian in the Precambrian exposure of Southwestern Nigeria. Journal of Mining and Geology, 34, 194 -197.

Anderson, N. L., 2006. Selection of Appropriate Geophysical Techniques: A Generalized Protocol Based on Engineering Objectives and Site Characteristics. Proc., 2006 Highway NDE Conference, 2006, 29–47. http://2006geophysics.mst.edu/.

Bufford, K. M., Atekwana, E. A. and Abdelsalam, M. G., 2012. Geometry and faults tectonic activity of the Okavango Rift Zone, Botswana: evidence from magnetotelluric and electrical resistivity tomography imaging. Journal of African Earth Sciences, 65, 61–71.

Chavez, R. E., Cifuentes-Nava, G., Tejero, A., Hernandez-Quintero, J. E. and Vargas, D., 2014. Special 3D electric resistivity tomography (ERT) array applied to detect buried fractures on urban areas: San Antonio Tecomitl, Milpa Alta, Mexico. Geofisica Internacional 53(4), 425-434

Cosenza, P., Marmet, E., Rejiba, F., Cui, Y. J., Tabbagh, A. and Charlery, Y., 2006. Correlations between geotechnical and electrical data: A case study at Garchy in France, Journal of Applied Geophysics, 60(3), 165–178

El-Qady, G., Hafez, M., Abdalla, M. A. and Ushijima, K., 2005. Imaging subsurface cavities using geoelectric tomography and ground penetrating radar, Journal of Cave and Karst Studies, 67(3), 174–181.

Ekwe, A., Opara, A. and Onwuka, O., 2018. Geoelectrical study of corrosivity and competence of soils within Uburu and Okposi areas of Ebonyi State, Southeastern Nigeria", Anti-Corrosion Methods and Materials, 65(6), 637-645.

Frid, V., Liskevich, G., Doudkinski, D. and Korostishevsky, N., 2008. Evaluation of landfill disposal boundary by means of electrical resistivity imaging. Environmental Geology, 53(7), 1503–1508.

LaBrecque, D. J., Ramirez, A. L., Daily, W, D., Binley, A. M. and Schima, S. A., 1996. ERT monitoring of environmental remediation processes," Measurement Science and Technology, 7(3), 375–383.

Lines, J. P., Bernardes, S., He, J., Zhang, S., Bacchus, S. T., Madden, M. and Jordan, T., 2012. Preferential Groundwater Flow Pathways and Hydroperiod Alterations Indicated by Georectified Lineaments and Sinkholes at Proposed Karst Nuclear Power Plant and Mine Sites. Journal of Sustainable Development, 5(12), 78-116.

Mohamed, N. E., Brasse, H., Abdelgalil1, M. Y. and Kheiralla, K. M., 2012 Geoelectric and VLF electromagnetic survey on complex aquifer structures, Central Sudan. Comunicacoes Geologicas 99(2): 95-100.

Moisidi, M., Vallianatos, F., Soupios, P., Kershaw, S., Rust, D. and Piscitelli, S., 2013. Modelling tectonic features of the Kissamos and Paleohora areas, Western Crete (Greece): combining geological and geophysical surveys. Journal of Geophysics and Engineering, 10(2), Article ID 025015.

Odeyemi I. B., 1988. Lithostratigrahic and structural relationship of the upper Precambrian metasediments of the Igarra area, Southwestern Nigeria. In: Oluyide, P. O., Mbonu, W. C., ogezi, A. E., Egbnike, I. G., Ajibade, A. C., Ana-Umeji, A. C. (Eds.) Precambrian geology of Nigeria. Geological Survey Nigeria Publication, Kaduna, 111-123.

Ogbe, O. B., Olobaniyi, S. B., Ejeh, O. I., Omo-Irabor, O. O., Osokpor, J., Ocheli, A. and Overare, B., 2018. Petrological and structural investigation of rocks around Igarra, Southwestern Nigeria. Ife Journal of Sciences, 20(3), 663 – 677.

Park, S. K. and Roberts, J. J., 2003. Conductivity structure of the San Andreas fault, Parkfield, revisited. Geophysical Research Letters, 30(16), 1842, doi:10.1029/2003GL017689, 2003.

Rahaman, M. A., 1989. Review of the Basement Geology of South-Western Nigeria. In: C. A. Kogbe (Ed), Geology of Nigeria, Nigeria: Rock View Limited), 39-56.

Rizzo, E., Colella, A., Lapenna, V. and Piscitelli, S., 2004. High-resolution images of the fault-controlled High Agri Valley basin (Southern Italy) with deep and shallow electrical resistivity tomographies. Physics and Chemistry of the Earth, 29(4–9), 321–327.

Robineau, B., Join, J. L., Beauvais, A., Parisot, J-C. and Savin, C., 2007. Geoelectrical imaging of a thick regolith developed on ultramafic rocks: groundwater influence," Australian Journal of Earth Sciences, 54(5), 773–781.

Soupios, P. M., Georgakopoulos. P., Papadopoulos, N., Saltas, V., Andreadakis, A., Vallianatos, F., Sarris, A. and Makris, J. P., 2007. Use of engineering geophysics to investigate a site for a building foundation, Journal of Geophysics and Engineering, 4(1), 94–103.

Turner, D. C., 1989. Upper Proterozoic Schist Belts in the Nigerian Sector of the Pan-African Province of West Africa. In: C. A. Kogbe (Ed), Geology of Nigeria, Nigeria: Rock View Limited), 93-109.

Twiss, R. J. and Moore, E. M., 2007: Structural Geology. W. H. Freeman and Company, New York. Second Edition. P. 736.

Unsworth, M. J., Malin, P. E., Egbert, G. D. and Booker, J. R., 1997. Internal structure of the San Andreas fault at Parkfield, California, Geology, 25, 359– 362.

Yassin, R. R., Muhammad, R. F., Taib, S. H. and Al-Kouri, O., 2014. Application of ERT and Aerial Photographs Techniques to Identify the Consequences of Sinkholes Hazards in Constructing Housing Complexes Sites over Karstic Carbonate Bedrock in Perak, Peninsular Malaysia. Journal of Geography and Geology, 6(3), 55-89.

Yi, M. J. and Kim, J. H., 1998. Enhancing the resolving power of the least squares inversion with Active Constraint Balancing: SEG Expanded Abstracts, 68 Annual Meeting, New Orleans, 485-488.

Zume, J. T., Tarhule, A. and Christenson, S., 2006. Subsurface imaging of an abandoned solid waste landfill site in Norman, Oklahoma. Groundwater Monitoring and Remediation, 26(2), 62–69.